Regenerative Therapy 28 (2025) 51–62

Contents lists available at ScienceDirect

Regenerative Therapy

journal homepage: http://www.elsevier.com/locate/reth

Original Article

Nanocurcumin-enhanced zein nanofibers: Advancing macrophage polarization and accelerating wound healing

Mohammad Ebrahim Astaneh [a, b, c], Narges Fereydouni [b, c, d, *]

[a] Department of Anatomical Sciences, School of Medicine, Fasa University of Medical Sciences, Fasa, Iran
[b] Department of Tissue Engineering, School of Medicine, Fasa University of Medical Sciences, Fasa, Iran
[c] Student Research Committee, Fasa University of Medical Sciences, Fasa, Iran
[d] Noncommunicable Diseases Research Center, Fasa University of Medical Sciences, Fasa, Iran

ARTICLE INFO

Article history:
Received 5 October 2024
Received in revised form
10 November 2024
Accepted 20 November 2024

Keywords:
Curcumin
Nanofibers
Macrophage polarization
Inflammatory cytokines
Wound healing

ABSTRACT

Introduction: Chronic wounds continue to pose a significant global challenge, incurring substantial costs and necessitating extensive research in wound healing. Our previous work involved synthesizing zein nanofibers embedded with 5 %, 10 %, and 15 % nano-curcumin (Zein/nCUR 5, 10, and 15 % NFs), and examining their physicochemical and biological properties. This study aims to explore the potential of these nanofibers in macrophage (MØ) polarization and wound healing.

Methods: We assessed the survival of RAW264.7 cells cultured on Zein/nCUR 5, 10, and 15 % NFs using the MTT assay. To evaluate MØ polarization, we measured the expression of iNOS and Arg-1 genes in MØs cultured on Zein/nCUR 10 % NFs through real-time PCR. Furthermore, we examined the nanofibers' impact on pro-inflammatory cytokine expression (IL-1β, IL-6, TNF-α) in MØs via real-time PCR. The wound healing efficacy of Zein/nCUR 10 % NFs was tested on 54 male rats with full-thickness wounds, with assessments conducted on days 3, 7, and 14. Wound closure, re-epithelialization, and collagen secretion were evaluated through photographic analysis and tissue staining. Statistical analyses were performed using GraphPad Prism 6, with significance set at $p < 0.05$.

Results: Zein/nCUR 10 % NFs significantly enhanced the survival of RAW264.7 cells compared to other groups. They also markedly reduced iNOS expression and increased Arg-1 expression, indicating successful polarization of M1 to M2 MØs. Additionally, these nanofibers decreased the expression of IL-1β, IL-6, and TNF-α, and significantly improved wound closure, re-epithelialization, and collagen deposition compared to control and Zein groups.

Conclusions: This study demonstrates that Zein/nCUR 10 % NFs effectively polarize MØs from M1 to M2, significantly enhancing wound healing, thus offering a promising therapeutic approach for improved wound care.

1. Introduction

Wound healing is a meticulously regulated process that involves a sequence of distinct cellular and molecular phases, including hemostasis, inflammation, proliferation, and remodeling [1]. A crucial determinant of successful wound healing is the transition from the inflammatory phase to the proliferative phase. This transition is heavily influenced by MØs, which play a pivotal role in modulating the wound environment [2]. MØs, upon activation by specific environmental cues, can differentiate into two main subtypes: the proinflammatory M1 MØs and the anti-inflammatory, wound-healing M2 MØs. Effective wound repair relies on the timely phenotypic switch from M1 to M2 MØs [2]. This switch is essential as M1 MØs are important for initial pathogen defense and inflammation, but their prolonged presence can hinder healing. In contrast, M2 MØs facilitate tissue repair and regeneration [3]. Current therapeutic strategies often focus on enhancing M2 MØ activity, recruiting additional M2 MØs, or introducing exogenous

* Corresponding author. Noncommunicable Diseases Research Center, Fasa University of Medical Sciences, Fasa, Iran.
E-mail address: n.fereydouni@fums.ac.ir (N. Fereydouni).
Peer review under responsibility of the Japanese Society for Regenerative Medicine.

https://doi.org/10.1016/j.reth.2024.11.016

M2 MØs into the wound site. However, these approaches frequently overlook the need to reduce or resolve the presence of persistent M1 MØs [3]. Failure to address the continuous presence of M1 MØs can lead to chronic inflammation and suboptimal healing. Thus, achieving a balanced MØ response that includes both the promotion of M2 MØs and the resolution of M1 MØs is critical for effective wound healing. This balance ensures a proper transition from inflammation to proliferation, ultimately leading to better wound healing outcomes [2–4].

Curcumin, the principal bioactive compound derived from turmeric, is renowned for its wide array of therapeutic properties, including anti-inflammatory, antioxidant, anti-cancer, and immune-modulatory effects [5]. These beneficial attributes have been substantiated through extensive laboratory research and numerous clinical trials. Curcumin's multifaceted roles in promoting health and combating disease have positioned it as a significant natural compound in both traditional and modern medicine [5,6]. Despite these beneficial properties, curcumin's therapeutic potential is significantly hindered by its hydrophobic nature, poor water solubility, low stability, and rapid metabolism [7]. To address these limitations, advanced drug delivery systems have been developed to enhance curcumin's solubility and metabolic stability [8,9]. One promising approach involves the incorporation of curcumin into nanofibrous (NFs) scaffolds [10]. Researchers have engineered various wound dressing nanocomposites containing curcumin-loaded NFs to study their physicochemical properties, curcumin release profiles, and effects on wound healing. These studies suggest that curcumin-loaded NFs may promote wound healing by maintaining curcumin's antioxidant, anti-inflammatory, and antibacterial properties, alongside the beneficial characteristics of the polymer scaffolds [11–16].

Our previous research was pioneered an oil-in-water (O/W) nanoemulsion form of curcumin embedded in a zein nanofibrous scaffold, evaluating its physicochemical and biological properties [17]. Building on this work, the current study aims to explore the potential of this unique nanofiber system to facilitate the transition of RAW264.7 macrophages from the proinflammatory M1 phenotype to the anti-inflammatory M2 phenotype, ultimately enhancing wound healing processes. This study presents a novel approach by focusing on the modulation of macrophage phenotypes using nanocurcumin within a scaffold designed to improve its bioavailability and efficacy in wound healing applications. By linking the physicochemical properties of the zein/nCUR nanofibers to their biological effects, we hypothesize that these nanofibers not only support the controlled release of curcumin but also facilitate the modulation of the wound environment through macrophage polarization, ultimately promoting faster and more effective wound healing.

2. Material and methods

2.1. Preparation of Zein and Zein/nCUR NFs

The synthesis of nano-curcumin (nCUR), preparation of Zein solutions, and subsequent fabrication of nanofibers were conducted following protocols established in a previous study. Briefly, nCUR was synthesized using an oil-in-water emulsion method [18]. The nCUR was mixed at concentrations of 5 %, 10 %, and 15 % (v/v) into a 25 % (w/w) Zein solution and stirred for 12 h to achieve a homogeneous mixture, with a blank Zein solution prepared for comparison. Electrospinning was employed to fabricate both Zein nanofibers (Zein NFs) and Zein nanofibers incorporating nCUR (Zein/nCUR NFs) using an electrospinning machine (model ES1000, Fanavaran Nanomeghyas Co., Iran) equipped with a high voltage power supply (0–30 kV). The 5 ml plastic syringes were filled with the respective solutions and connected to a 16-gauge stainless steel needle. The solutions were dispensed at a rate of 2.5 ml/h under a voltage of 25 kV, with the distance between the needle and the collector set at 150 mm. The nanofibers were then collected on a rotating collector covered with aluminum foil [17].

2.2. Cell culture

The murine MØ cell line RAW264.7, obtained from the Pasteur Institute of Iran (NCBI Code: C639), was cultured in DMEM supplemented with 10 % fetal bovine serum (FBS) and 1 % penicillin-streptomycin. These cells were incubated at 37 °C in a humidified atmosphere containing 5 % CO2. To promote the M1 phenotype in RAW264.7 MØs, cells were exposed to lipopolysaccharide (LPS) at a concentration of 100 ng/ml along with interferon-gamma (IFN-γ) at a concentration of 10 ng/ml over a duration of 48 h. For MØ seeding on the nanofibers, the nanofibers were first cut into circular disks and sterilized under UV radiation overnight on both sides in a laminar flow hood. The disks were then washed three times with PBS and immersed in DMEM overnight before cell seeding. This immersion step was crucial to enhance cell attachment to the nanofiber surfaces.

2.3. Viability assay

For the MTT assay, RAW264.7 cells were seeded onto the surface of Zein and Zein/nCUR 5 %, 10 %, and 15 % NF disks at a density of 10^5 cells per well. The plates were incubated in a humidified environment with 5 % CO2 at 37 °C. The viability of the cells adhered to the nanofibrous mats was evaluated using the MTT assay on days 1 and 3 of culture. The experiment was repeated three times, and the results were expressed as the mean ± standard deviation (SD) for evaluation.

2.4. Quantitative real-time PCR assay

To evaluate the *in vitro* efficacy of Zein and Zein/nCUR 5 %, 10 %, and 15 % NFs in modulating MØ polarization from the M1 to the M2 phenotype, changes in the expression levels of M1 marker iNOS2 and M2 marker Arg1 were assessed in M1 MØs after three days of incubation using real-time PCR. Additionally, the expression levels of pro-inflammatory cytokines TNF-α, IL-1β, and IL-6 were measured. For this purpose, Zein and Zein/nCUR NFs were seeded with M1 MØs at a density of 5×10^4 cells per well in 6-well plates and incubated for 72 h at 37 °C. Total RNA was then extracted using the Trizol RNA extraction kit (Yectatajhiz), and RNA concentration was determined by measuring absorbance at 260 and 280 nm with a nanodrop apparatus (Synergy HTX Multi-Mode Reader, USA). Approximately 2 μg of RNA was reverse-transcribed into cDNA using a cDNA synthesis kit (Yectatajhiz, Iran). Amplification was performed with RealQ Plus 2x Master Mix Green high ROX™ (Amplicon, Denmark) on a qPCR machine (StepOnePlus, Applied Biosystems, USA). The reaction mixture, consisting of the master mix, forward and reverse primers for each gene (Pishgam Biotech Co., Tehran, Iran), and cDNA template, was adjusted to a final volume of 20 μL using DEPC water. The amplification protocol included an initial denaturation step at 95 °C for 10 min, followed by 40 cycles of 95 °C for 15 s, 55 °C for 30 s, and 72 °C for 30 s. Relative fold changes in target gene expression, normalized to the β-actin gene as an internal control, were calculated using the $2-\Delta\Delta CT$ method, where ΔCT is the difference between the threshold cycles of the target and reference genes, and ΔΔCT is the difference between ΔCT values of the test and control samples. The experiment was repeated three times, and the results were expressed as the mean ± SD for evaluation.

2.5. Animal studies

Fifty-four male Wistar rats, weighing between 200 and 250 g and aged between 8 and 10 weeks, were acquired from the animal facility at Fasa University of Medical Sciences. Male rats were chosen to reduce variability in wound healing due to hormonal fluctuations typically associated with the female reproductive cycle, ensuring more consistent and stable data. All rats were housed in standard polystyrene cages under controlled conditions, including a 12-h light/dark cycle, a stable temperature of 25 ± 2 °C, controlled humidity, and unrestricted access to food and water. All experimental procedures were approved by the Bioethics Committee of Fasa University of Medical Sciences (Ethics code: IR.FUMS.REC.1399.121). The study adhered to ARRIVE (Animal Research: Reporting of In Vivo Experiments) 2.0 guidelines to ensure transparency, ethical practices, and reproducibility of the research, and a completed ARRIVE checklist has been included as supplementary material. Furthermore, all procedures were conducted following the standards of the Animals (Scientific Procedures) Act 1986 and the EU Directive 2010/63.

Rats were randomly divided into three groups: Control, Zein NFs, and Zein/nCUR 10 % NFs, with six rats in each group evaluated at 3, 7, and 14 days post-surgery. To minimize inter-animal variability, randomization was implemented at the beginning of the study. The rats were anesthetized using intraperitoneal injections of ketamine (100 mg/kg) and xylazine (10 mg/kg). After achieving adequate anesthesia, the hair on the rats' backs was shaved and the area disinfected using 70 % alcohol.

A 2 × 2 cm full-thickness excisional wound was created on the mid-back of each rat using a sterile razor and surgical scissors [19,20]. The wound size was consistently marked across all rats using a template to ensure uniformity, though minor variations due to human error were addressed by photographing the wounds from a fixed distance at designated time points for accurate wound closure analysis. Digital images of the wounds were captured on days 0, 3, 7, and 14 to calculate the percentage of wound closure based on the initial wound area at day 0.

Immediately following surgery, the designated treatment (Zein NFs or Zein/nCUR 10 % NFs) was applied to the wound once on day 0. The nanofiber scaffolds were carefully placed on the wound surface and then secured with a sterile bandage to ensure that the treatment remained in place. The bandages were kept in place throughout the study to prevent contamination and to allow the nanofibers to interact with the wound for optimal healing. The control group received no treatment but had the wound similarly covered with sterile bandages. No additional applications of nanofibers were made after the initial placement.

To prevent bias during data collection and analysis, blinding was implemented. The researcher conducting the analysis of wound healing outcomes, including measurements of wound closure percentages and histological assessments, was not informed of the treatment groups during the analysis phase.

Wounds were photographed on days 0, 3, 7, and 14 for macroscopic evaluation of wound healing. The percentage of wound closure was calculated by comparing the wound area at each time point to the initial wound area measured on day 0. After 7 and 14 days post-wounding, rats were sacrificed, and the wound tissues were harvested. The excised tissues included a 2 mm margin of healthy skin surrounding the wound and were fixed in 10 % formalin for subsequent histological analysis.

2.6. Macroscopic wound closure

To assess wound closure on days 3, 7, and 14, photographs of the wounds were taken from a consistent distance. The wound area was measured using ImageJ software, and the wound closure rate was calculated using the following equation [21].

$$\textit{Wound closure}\ (\%) = \frac{(A_o - A_x)}{A_o} \times 100$$

where A_0 is the wound area on day zero, and A_x is the wound area on days 3, 7, and 14. The percentage of wound closure for each group was determined with 5 replicates, and the results were reported as mean ± standard error (SE). The experiment was repeated five times, and the results were expressed as the mean ± SD for evaluation.

2.7. Histological staining

Immediately following euthanasia, the wound along with a 2 mm margin of surrounding tissue was excised at full thickness and fixed in 10 % formalin for 3 day at room temperature. The skin samples were then embedded in paraffin blocks, sectioned into 5-μm thick slices, and mounted on glass slides. These sections underwent standard histological staining procedures, including hematoxylin and eosin (H&E) and Masson's trichrome (MT) staining. The stained slides were subsequently photographed using a light microscope equipped with a Canon EOS camera. The intensity of the blue color in the trichrome-stained sections, which indicates the amount of collagen deposited at the wound site, was scored by a pathologist experienced in wound healing, using ImageJ software for quantitative analysis. The scoring system ranged from 0 to 3, with 0 indicating very low collagen secretion, 1 indicating low collagen secretion, 2 indicating moderate collagen secretion, and 3 indicating high collagen secretion. The experiment was repeated three times, and the results were expressed as the mean ± SD for evaluation.

2.8. Histological analysis

Re-epithelialization was analyzed using ImageJ software on microscopic images taken at 40X magnification from both sides of the wound on samples collected on the 7th and 14th days. The percentage of re-epithelialization was calculated using the following equation [21].

$$\textit{Percentage of re}-\textit{epithelialization}\ (\%) = \frac{\text{Length of newly formed epithelium}}{\textit{Total wound length}} \times 100$$

This method allowed for precise measurement and analysis of the extent of re-epithelialization in the wound healing process over time. Additionally, to measure the thickness of the new epithelium, images taken from the tissue slides at 40X magnification from both sides of the wound on samples collected on the 14th day were used. The thickness of the neoepithelium was determined and measured at three different points—left, right, and middle of the wound—using ImageJ software, offering a detailed evaluation of the wound healing process. The experiment was repeated three times, and the results were expressed as the mean ± SD for evaluation.

2.9. Statistical analysis

Statistical analyses were performed using GraphPad Prism 6.0 software. Data normality was assessed using the Kolmogorov–Smirnov test. For comparisons involving more than two groups, mean ± SE values were analyzed using a one-way ANOVA, followed by post-hoc Tukey tests to determine significant

differences between groups. For non-parametric data, the Kruskal–Wallis test was employed to evaluate group differences. A significance level of $p < 0.05$ was considered statistically significant.

3. Results

3.1. In vitro properties of nanofibers

In our previous study, we investigated the physicochemical properties of Zein and Zein/nCUR NFs with 5 %, 10 %, and 15 % nCUR concentrations. Parameters such as viscosity, field emission scanning electron microscopy (FESEM), Fourier-transform infrared spectroscopy (FTIR), tensile strength, pore size, encapsulation efficiency, release profile, water vapor transmission rate (WVTR), and water uptake capacity were thoroughly examined. Additionally, we assessed the biological properties, including cytotoxicity and antioxidant activity. Our findings revealed that optimal electrospinning parameters were achieved, resulting in the production of uniform, bead-free nanofibers. We observed a significant decrease in the mean diameter of Zein NFs and an improvement in mechanical properties with increased nCUR content. The nanofibers with higher nCUR percentages demonstrated greater *in vitro* release and lower encapsulation efficiency compared to other groups. Notably, the Zein/nCUR 10 % NFs provided the most favorable conditions for cell proliferation based on viability and antioxidant assessments.

3.2. Viability assay

The viability of RAW264.7 cells cultured on Zein and Zein/nCUR 5 %, 10 %, and 15 % NFs concentrations was assessed using the MTT assay at 24 and 72 h. As illustrated in Fig. 1, cell viability peaked in the Zein/nCUR 10 % NFs group, showing a significant increase compared to the control and Zein groups on the first day. By the third day, the Zein/nCUR 10 % NFs group exhibited significantly higher cell viability than the control, Zein, and Zein/nCUR 5 % NFs groups. Although the Zein/nCUR 10 % NFs showed greater cell proliferation than the 5 % and 15 % NFs on the first day, this difference was not statistically significant. On the third day, however, the Zein/nCUR 10 % NFs displayed significantly higher viability than the Zein/nCUR 15 % NFs. These results guided the selection of the Zein/nCUR 10 % NFs group for subsequent studies due to its superior performance in promoting cell proliferation.

3.3. In vitro repolarization study

To assess the effectiveness of Zein/nCUR nanofibers (NFs) in repolarizing RAW264.7 MØs from the M1 to M2 phenotype, we employed real-time PCR to measure the expression levels of the iNOS and Arg-1 genes in M1 MØs cultured on Zein and Zein/nCUR 10 % NFs for 72 h (Fig. 2). The iNOS gene was used as an M1 marker, while Arg-1 served as an M2 marker to evaluate the repolarization potential of the MØs on the nanofibers containing nCUR. As depicted in Fig. 2, LPS/IFN-γ stimulation resulted in a 450-fold increase in iNOS levels in MØs cultured in the control group, confirming successful polarization to the M1 phenotype. The presence of nCUR in Zein NFs significantly reduced the iNOS level to 103-fold in MØs compared with a 437-fold increase observed in the Zein NFs group ($p < 0.0001$), indicating that Zein NFs alone did not significantly affect iNOS expression. In contrast, the expression level of Arg-1 in MØs cultured on Zein/nCUR 10 % NFs significantly increased to 197-fold, whereas Zein NFs alone did not significantly affect Arg-1 levels (44-fold), showing no significant difference from the control group. These findings demonstrate that RAW264.7 MØs were effectively repolarized from the M1 to M2 phenotype when cultured on Zein/nCUR 10 % NFs.

3.4. Anti-inflammatory effect of Zein/nCUR 10 % NFs

After inducing the switch of MØ phenotype to the M2 type on Zein/nCUR 10 % nanofibers (NFs), we investigated the gene expression levels of three key proinflammatory cytokines involved in the inflammatory wound process: IL-6, IL-1β, and TNF-α. These cytokines were examined in M1 MØs cultured on Zein and Zein/nCUR 10 % NFs for three days (Fig. 3). As depicted in Fig. 3, LPS/IFN-γ stimulation significantly upregulated TNF-α, IL-1β, and IL-6 in MØs seeded on both the control and Zein NFs compared to untreated cells (Normal group). However, when MØs were cultured on Zein/nCUR 10 % NFs, there was a dramatic reduction in the expression levels of TNF-α, IL-1β, and IL-6 after three days. This indicates that

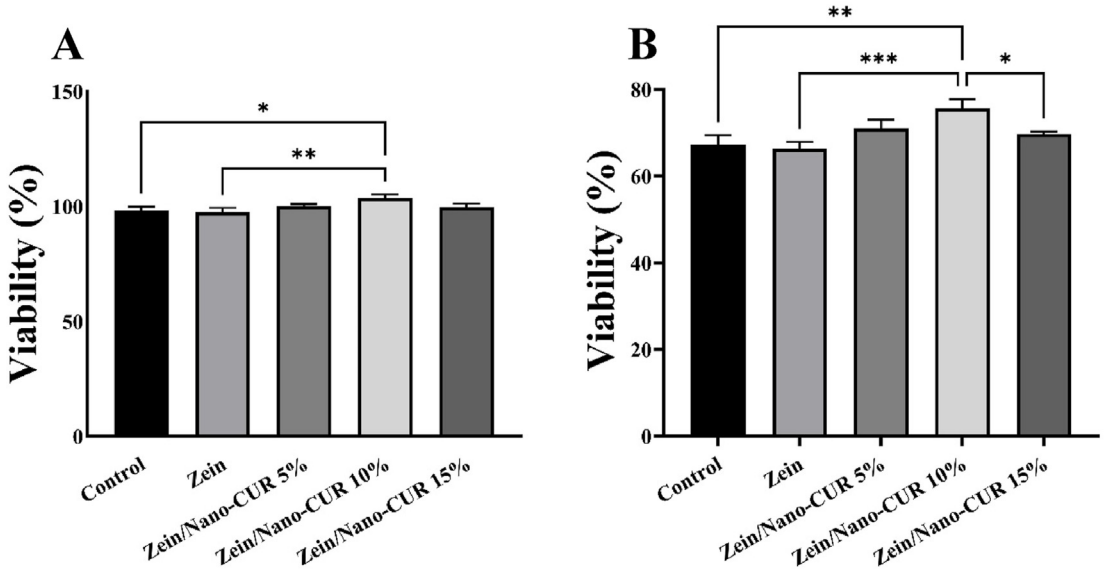

Fig. 1. Viability diagram of Zein and Zein/nCUR 5 %, 10 %, and 15 % NFs on RAW264.7 MØs on (A) 24 h, and (B) 72 h. The experiment was repeated three times, and the results were expressed as the mean ± SD for evaluation; (*$p < 0.05$, **$p < 0.01$, and ***$p < 0.001$).

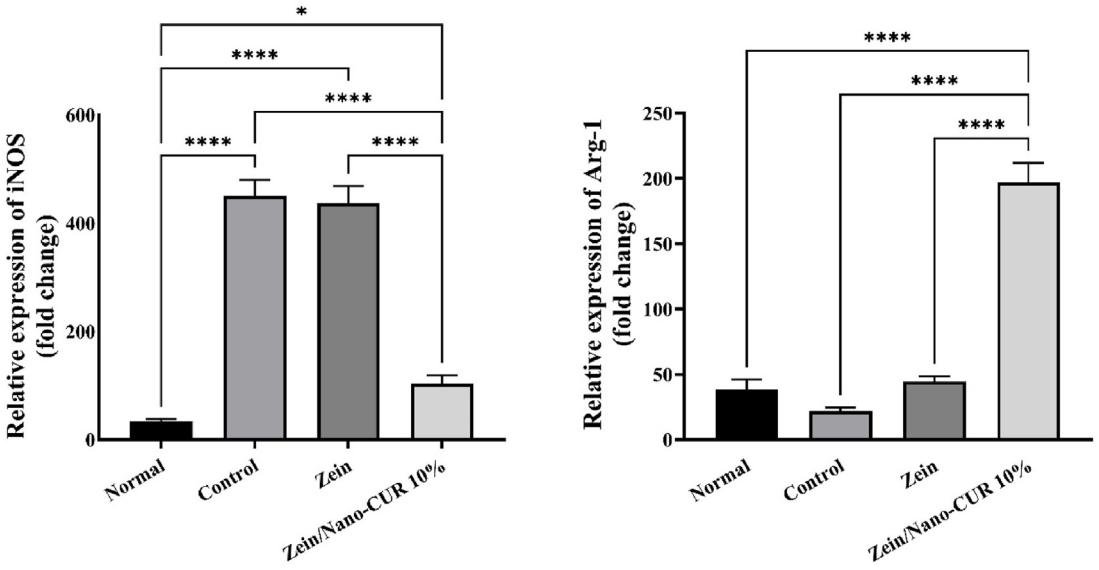

Fig. 2. Expression levels of iNOS (M1 marker) and Arg-1 (M2 marker) in M1 RAW264.7 MØs seeded on Zein and Zein/nCUR 10 % NFs for 72 h. The experiment was repeated three times, and the results were expressed as the mean ± SD for evaluation; (*$p < 0.05$, **$p < 0.01$, and ***$p < 0.001$).

the presence of nCUR effectively suppresses the inflammation induced by LPS/IFN-γ in the MØs, highlighting its potential for modulating inflammatory responses in wound healing.

3.5. Wound closure percentage

Figs. 4–6 displays macroscopic images of wounds treated with Zein NFs, Zein/nCUR 10 % NFs, and the control group, revealing no visible signs of inflammation or infection across all groups. The statistical analysis of wound closure percentages, illustrated in Fig. 7, indicates significant differences among the groups at various time points. On day 3, the wound closure percentages for the control, Zein NFs, and Zein/nCUR 10 % NFs were 3.7 ± 1.2 %, 12.6 ± 8.4 %, and 40.9 ± 11.4 %, respectively. By day 7, these values increased to 42.1 ± 9.9 % for the control group, 47 ± 12.3 % for the Zein NFs group, and 77.2 ± 15.4 % for the Zein/nCUR 10 % NFs group. By the 14th day, the wound closure percentages reached 89.3 ± 5.2 % for the control, 93.1 ± 2.4 % for the Zein NFs group, and 99.1 ± 0.5 % for the Zein/nCUR 10 % NFs group, demonstrating the superior wound healing efficacy of the Zein/nCUR 10 % NFs treatment.

3.6. Re-epithelialization

Figs. 8–10 presents the re-epithelialization observed in the control, Zein, and Zein/nCUR 10 % NFs groups on days 7 and 14, using H&E-stained slides at 40X magnification. The tissue sections reveal that new epithelial layers begin to form from the wound margins, progressively covering the wound area. On the seventh day, both the control and Zein NFs groups show initial epithelial advancement from the wound edges, which continues to progress by the fourteenth day but remains incomplete. In contrast, the Zein/nCUR 10 % NFs group displays significantly closer and more extensive epithelial coverage by the seventh day, with complete wound coverage by the fourteenth day. Fig. 11A illustrates that the percentage of re-epithelialization in the Zein/nCUR 10 % NFs group was significantly higher on both days 7 and 14 compared to the Zein NFs ($p < 0.001$) and control groups ($p < 0.001$), while no significant

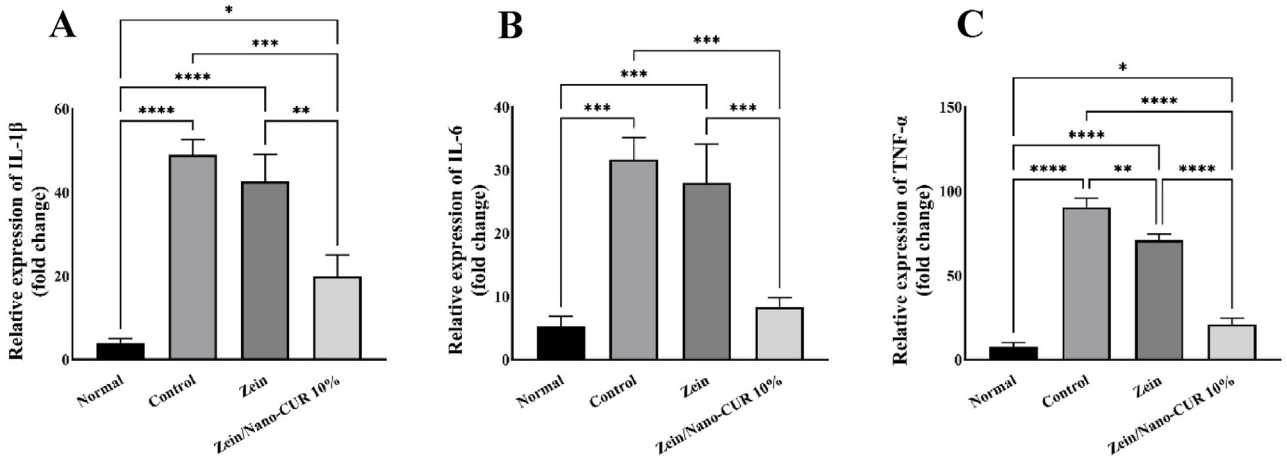

Fig. 3. Anti-inflammatory effect of Zein and 10 % Zein/nCUR NFs evaluated on RAW264.7 cells stimulated with LPS/IFN-γ. (A) IL-1b, (B) IL-6, and (C) TNF-a. The experiment was repeated three times, and the results were expressed as the mean ± SD for evaluation; (*$p < 0.05$, **$p < 0.01$, and ***$p < 0.001$).

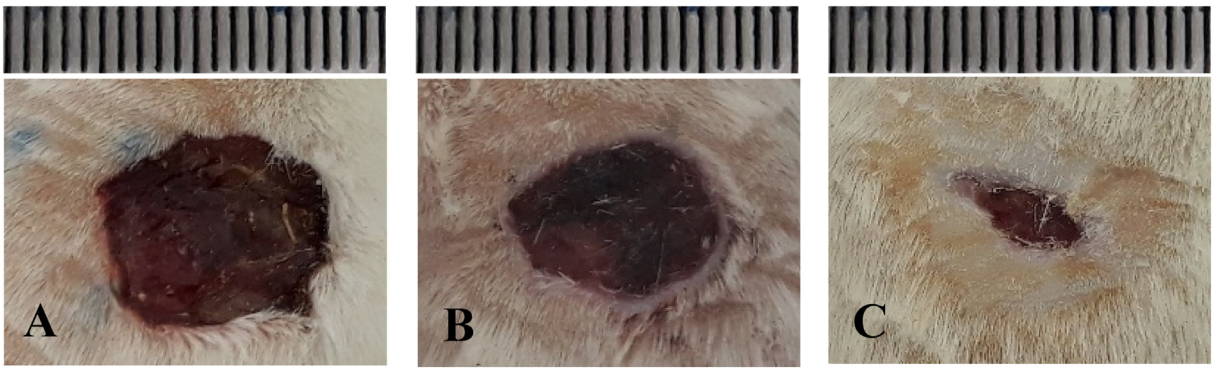

Fig. 4. Photograph images of wound closure of control group on days A) 3, B) 7, and C) 14. The distance between the lines in the ruler above is 1 mm.

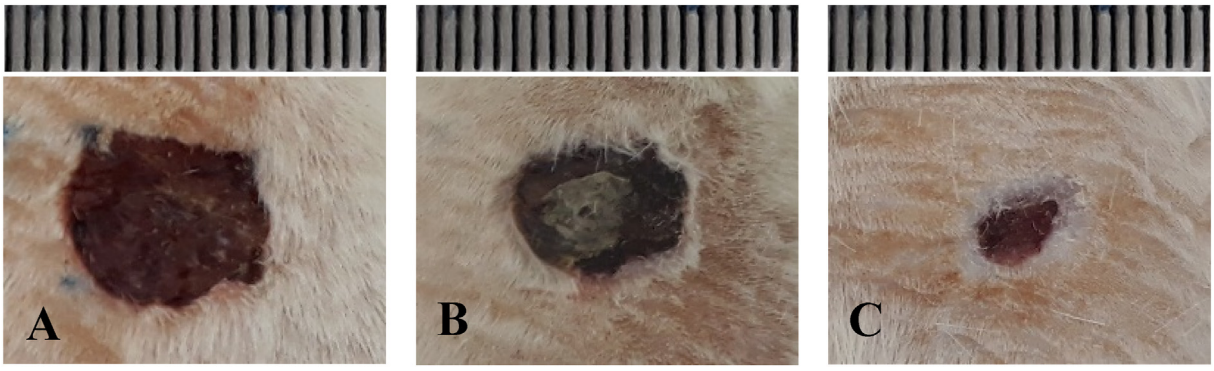

Fig. 5. Photograph images of wound closure of Zein NF group on days A) 3, B) 7, and C) 14. The distance between the lines in the ruler above is 1 mm.

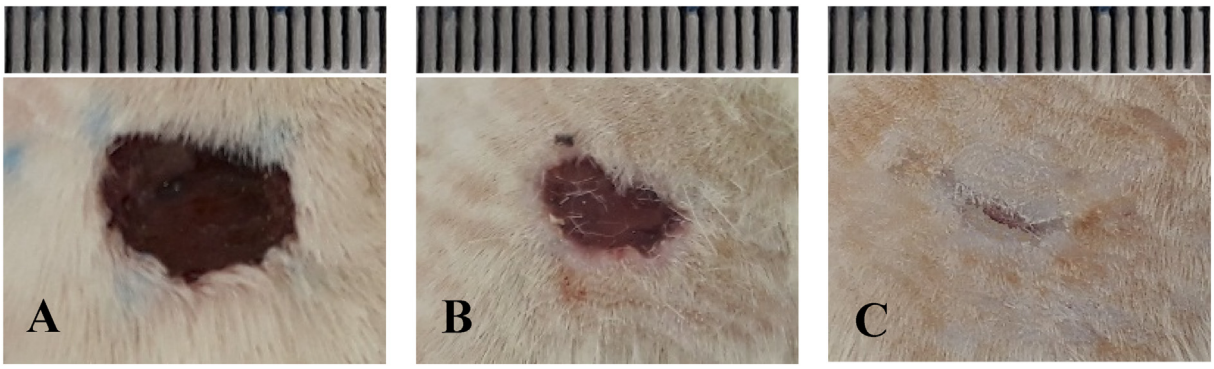

Fig. 6. Photograph images of wound closure of Zein/nCUR 10 % NF group on days A) 3, B) 7, and C) 14. The distance between the lines in the ruler above is 1 mm.

difference was observed between the Zein NFs and control groups. These results underscore the potent efficacy of nCUR in enhancing epithelial regeneration during wound healing. Additionally, Fig. 11B presents the thickness of the new epithelium measured on day 14 in the control, Zein, and Zein/nCUR 10 % NFs groups, as assessed using H&E-stained slides at 40X magnification. The data reveal that the epithelial thickness in the Zein/nCUR 10 % NFs group was significantly greater than in both the control ($p < 0.001$) and Zein groups ($p < 0.05$). Since increased epithelial thickness is a key marker of improved tissue regeneration, these findings suggest that Zein/nCUR 10 % NFs not only accelerate re-epithelialization but also promote the formation of a more robust epithelial layer, thus demonstrating its potential for enhancing wound healing outcomes.

3.7. Collagen content

Figs. 12–14 illustrates the collagen content in the control, Zein, and Zein/nCUR 10 % NFs groups on days 7 and 14, captured at 100X magnification. The intensity of the blue staining, indicative of collagen deposition at the wound site, was scored on a scale from 0 to 3. Subsequent statistical analysis of these scores, as depicted in Fig. 15, reveals that collagen secretion in the Zein/nCUR 10 % NFs group significantly increased on day 7 ($p < 0.01$) and day 14 ($p < 0.001$) compared to the control group. However, no significant difference in collagen secretion was observed between the Zein/nCUR 10 % NFs and Zein NFs groups. Similarly, the Zein NFs and control groups did not exhibit a significant difference in collagen deposition.

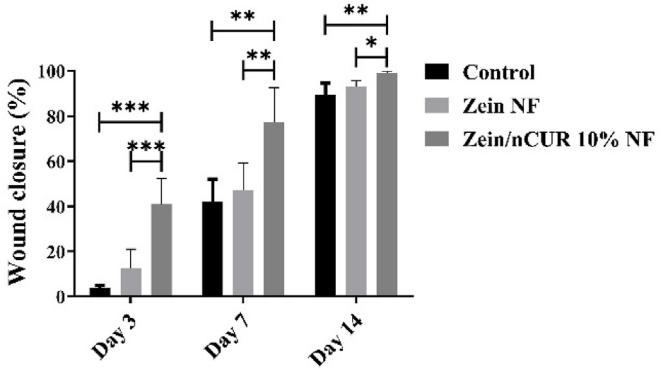

Fig. 7. Wound closure of the studied groups on days 3, 7, and 14. The experiment was repeated five times, and the results were expressed as the mean ± SD for evaluation. The star sign indicates the significant difference between the groups (*$p < 0.05$, **$p < 0.01$, ***$p < 0.001$).

4. Discussion

Building on our previous research where we synthesized Zein nanofibers using the electrospinning method with three different concentrations (5 %, 10 %, and 15 % v/v) of nano-curcumin solution [17], this study delves into the wound healing capabilities of these nanofibers. The hypothesis of this study is that Zein/nCUR 10 % NFs will enhance wound healing through modulating macrophage polarization from the M1 to M2 phenotype, reducing inflammation, and promoting tissue regeneration. In the earlier study, we assessed the physicochemical and biological properties of the nanofibers and identified the Zein/nCUR 10 % NFs as the most promising candidate for further wound healing investigations. In this current study, we evaluated the wound healing efficacy of these nanofibers and observed that the Zein/nCUR 10 % NFs significantly enhanced the survival of RAW264.7 MØ cells compared to the control and Zein NFs groups on day 7. Additionally, on the 14th day, these nanofibers improved cell viability compared to the control, Zein, and Zein/nCUR 15 % NFs groups, corroborating our earlier findings. We further explored the potential of Zein/nCUR 10 % NFs to modulate LPS/IFN-γ-stimulated RAW264.7 MØs from M1 to M2 phenotype by examining the expression levels of iNOS (M1 marker) and Arg-1 (M2 marker) genes. Results indicated a significant reduction in iNOS expression and a notable increase in Arg-1 expression compared to the control and Zein groups. To confirm these polarization effects, we also analyzed the expression of inflammatory genes IL-1b, IL-6, and TNF-a in MØs cultured on Zein/nCUR 10 % NFs, finding a significant decrease in these inflammatory markers. Finally, in a rat model, Zein/nCUR 10 % NFs demonstrated a significant reduction in wound size, enhanced re-epithelialization, increased epithelium thickness, and improved collagen secretion, underscoring their potential as an effective wound healing treatment.

Numerous studies over the years have explored the effects of turmeric extracts, and more recently, the active compound curcumin, in various modern formulations or combinations with other substances. These investigations have highlighted curcumin's diverse properties, including antibacterial, anti-inflammatory, and angiogenic effects, all of which are beneficial for wound healing [11,22,23]. Specifically, curcumin's role as an immunomodulatory agent capable of altering MØ polarization from the pro-inflammatory M1 phenotype to the anti-inflammatory M2 phenotype has been documented in various diseases [24]. However, there is a lack of studies directly investigating curcumin's effects on MØ polarization in wound healing models. For instance, Berbudi et al. (2021) demonstrated that curcumin can enhance wound healing by promoting M2 MØ polarization. Their study showed a significant increase in Arg-1 gene expression and the Arg-1/iNOS ratio in rats treated with a gel containing turmeric extract, compared to the control group, indicating improved excision wound healing [25]. These findings are consistent with our results. Conversely, a study by Dehghani et al. reported different outcomes. In their study, diabetic rats with full-thickness wounds treated with 1 % curcumin exhibited improved wound healing through new angiogenesis but did not show significant effects on MØ polarization and re-epithelialization compared to the control group [26]. The discrepancies between our findings and those of Dehghani et al. could be attributed to differences in curcumin formulation types, concentrations used, or the source of RNA extraction. In our study, iNOS and Arg-1 genes were extracted from RAW264.7 MØs, whereas Dehghani et al. extracted genes from the skin samples of diabetic rats.

Extensive evidence underscores the pivotal role of MØs as critical regulators throughout the various stages of wound healing. By adapting their phenotype in response to spatio-temporal cues, MØs are essential in each phase of the healing process [27,28]. Upon wound formation, blood clotting at the injury site triggers the recruitment of immune cells, particularly polymorphonuclear neutrophils (PMNs), marking the onset of the inflammatory phase. Following the rapid influx of PMNs, monocytes are recruited to the wound site where, influenced by micro-environmental signals such as hypoxia, bacterial products, and necrotic cells, they differentiate into M1 MØs. These M1 MØs perform crucial scavenging, phagocytosis, and antigen-presenting functions while releasing nitric oxide (NO), reactive oxygen species (ROS), and pro-inflammatory

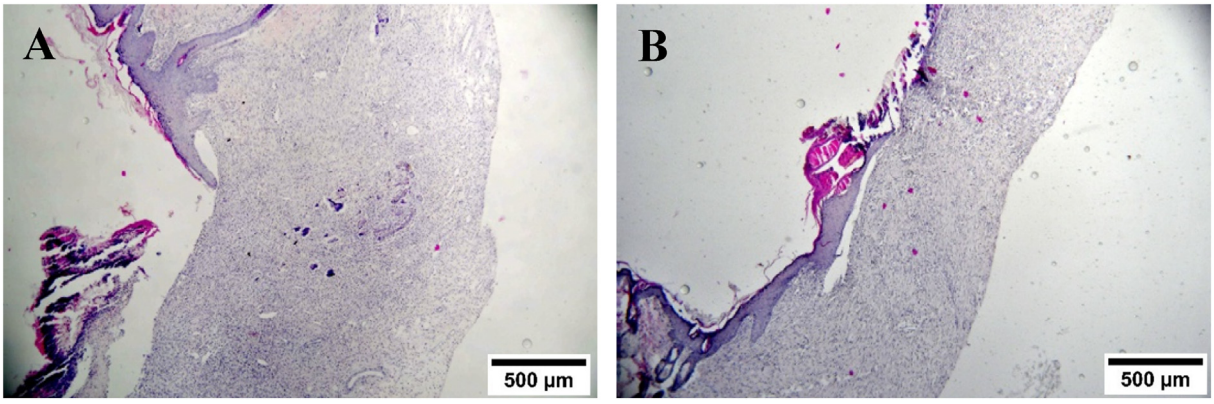

Fig. 8. Re-epithelialization in control group on days A) 7 and B) 14.

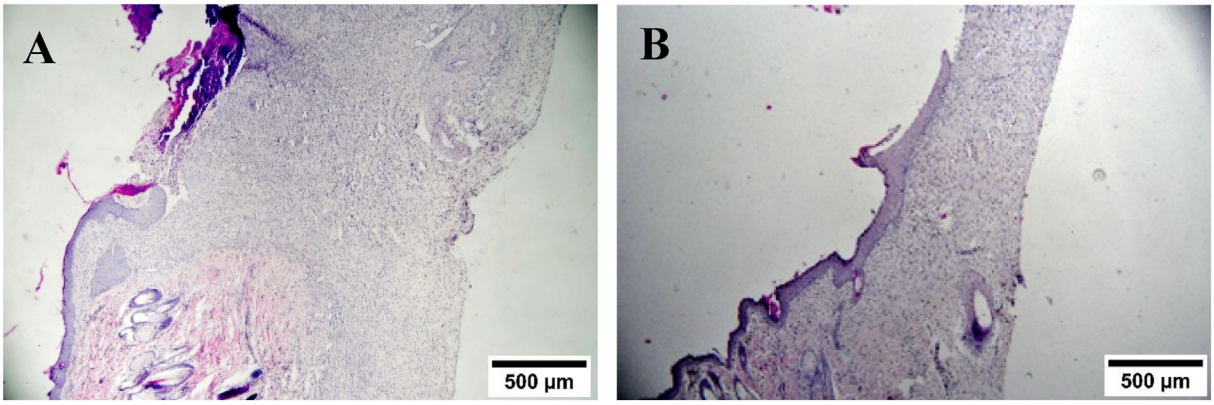

Fig. 9. Re-epithelialization in Zein NF group on days A) 7 and B) 14.

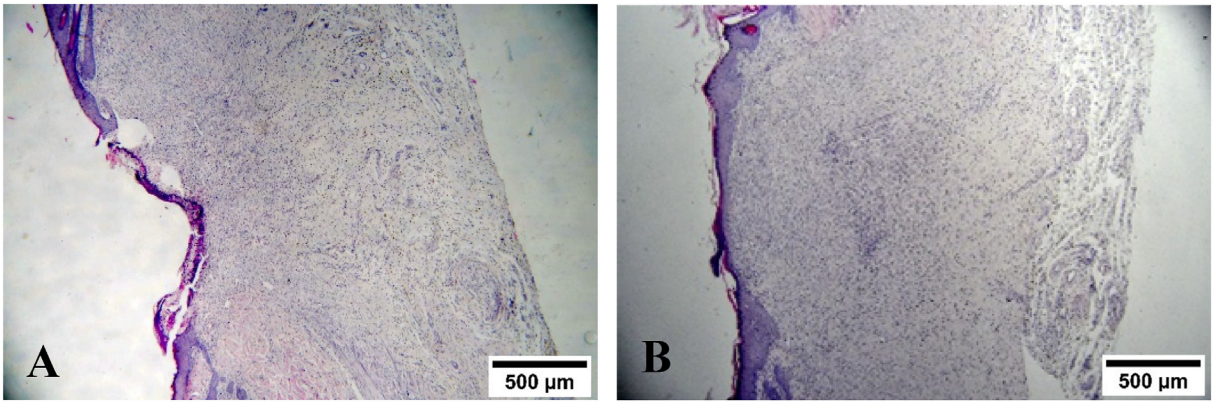

Fig. 10. Re-epithelialization in Zein/nCUR 10 % NF group on days A) 7 and B) 14.

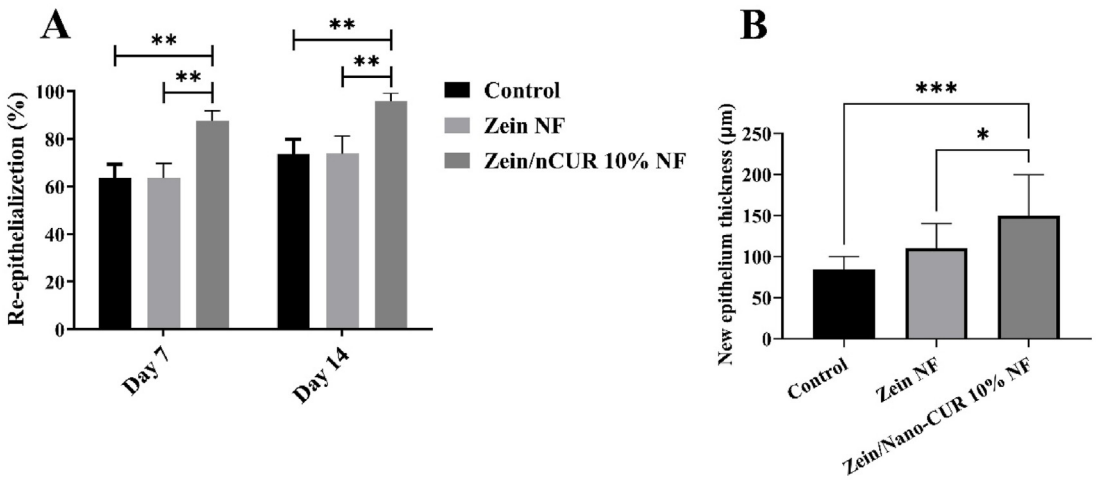

Fig. 11. A) Percentage of re-epithelialization on days 7 and 14, and B) New epithelium thickness on day 14 in the studied groups. The experiment was repeated three times, and the results were expressed as the mean ± SD for evaluation. The star sign indicates the significant difference between the groups (*$p < 0.05$, **$p < 0.01$, ***$p < 0.001$).

cytokines like TNF-α, IL-1α, IL-1β, IL-6, IL-12, and CXCL9/10, preparing the wound bed for subsequent healing stages [29,30]. As the wound stabilizes, provided there are no metabolic complications, MØs transition from the M1 to M2 phenotype, shifting their gene expression to secrete cytokines and growth factors that stimulate the proliferation, differentiation, and migration of endothelial cells, keratinocytes, and fibroblasts. This proliferative phase is characterized by MØs adopting a repair-oriented state, secreting reparative cytokines such as TGF-β, IL-10, PDGF, EGF, and VEGF [31]. In the final remodeling phase of wound healing, MØs continue to be instrumental by secreting matrix metalloproteinases, facilitating extracellular matrix deposition, particularly collagen, which reduces scar formation and restores the wound site's structural integrity [27].

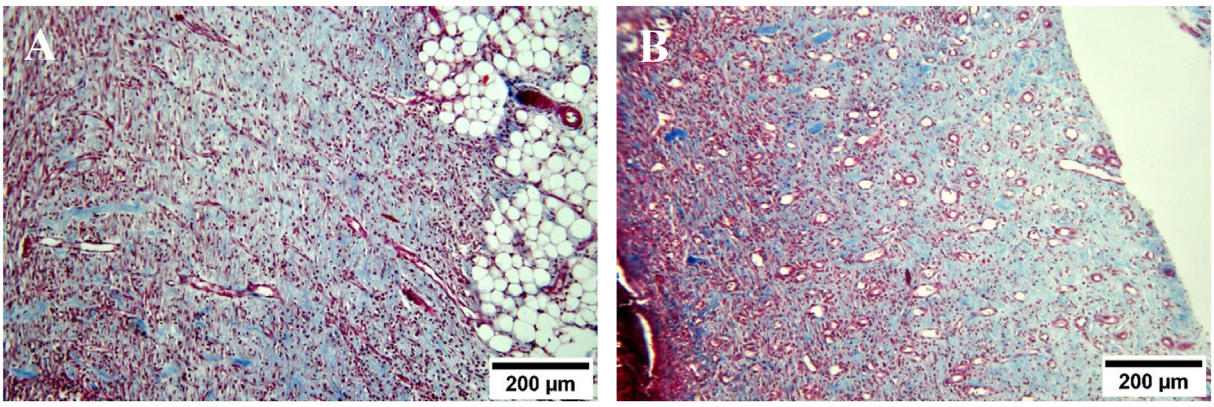

Fig. 12. Collagen content in control group on days A) 7 and B) 14 with masson's trichrome stain.

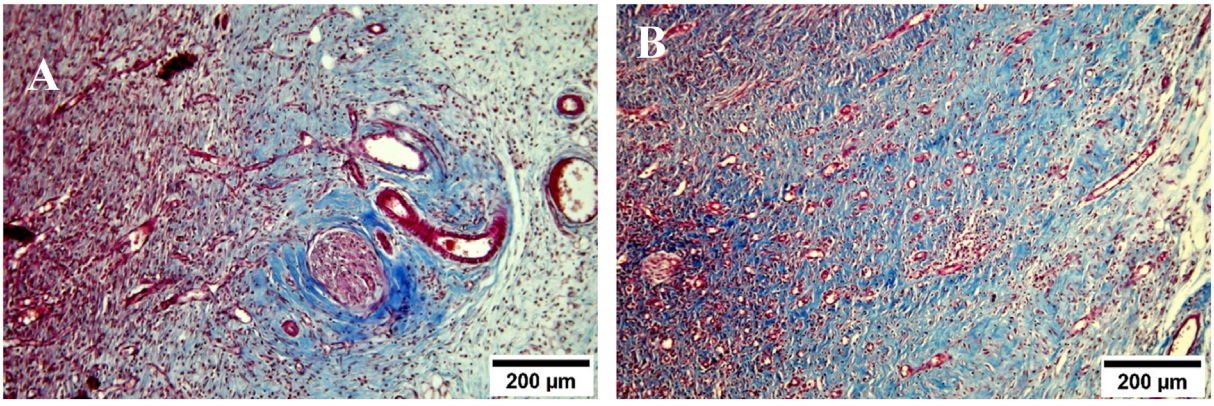

Fig. 13. Collagen content in Zein NF group on days A) 7 and B) 14 with masson's trichrome stain.

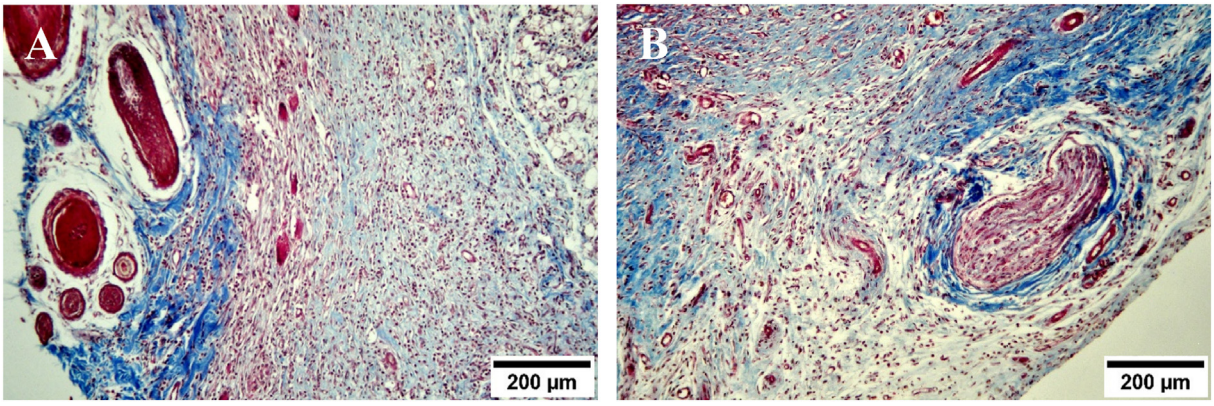

Fig. 14. Collagen content in Zein/nCUR 10 % NF group on days A) 7 and B) 14 with masson's trichrome stain.

Curcumin facilitates the polarization of MØs from the M1 to the M2 phenotype through multiple pathways. The primary mechanism involves the inhibition of the nuclear factor-kappa B (NF-κB) pathway, a crucial player in the activation of M1 MØs and the subsequent production of pro-inflammatory cytokines such as IL-1β, IL-6, and TNF-α. By suppressing NF-κB activity, curcumin significantly reduces the expression of these cytokines, thereby attenuating the M1 phenotype. This study corroborates these findings, demonstrating that Zein/nCUR 10 % nanofibers markedly decrease the levels of inflammatory cytokines IL-1β, IL-6, and TNF-α in RAW264.7 cells. Supporting this, Ran et al. found that curcumin mitigates microglial cell apoptosis induced by pro-inflammatory signals via the suppression of the NF-κB/NLRP3 pathway, consequently reducing white matter damage post-stroke [32]. Similarly, Lee et al. showed that curcumin pretreatment in MØs diminishes pro-inflammatory cytokine production induced by particulate matter through inactivation of the MAPK/NF-κB pathway [33]. Another vital mechanism is curcumin's activation of the peroxisome proliferator-activated receptor gamma (PPAR-γ), a nuclear receptor that fosters the M2 MØ phenotype. By activating PPAR-γ, curcumin promotes the transcription of anti-inflammatory genes while inhibiting pro-inflammatory cytokines, thus steering MØ

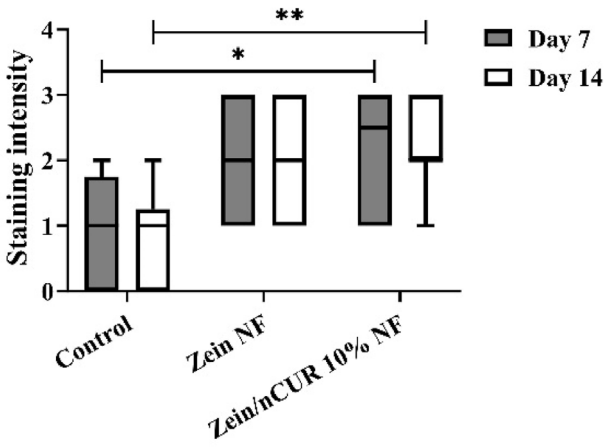

Fig. 15. Collagen content in the studied groups on days 7 and 14 with Masson's trichrome stain. The experiment was repeated three times, and the results were expressed as the mean ± SD for evaluation. The star sign indicates the significant difference between the groups (*$p < 0.05$, **$p < 0.01$, ***$p < 0.001$).

polarization towards the M2 phenotype. Chen et al. demonstrated that curcumin reduces inflammation induced by polylactic acid in foam cells via the PPAR-γ pathway [34]. Additionally, curcumin impacts the signal transducer and activator of transcription (STAT) pathways, particularly STAT1 and STAT3, which are central to mediating inflammatory responses [35,36]. By inactivating the JAK/STAT pathway, curcumin reduces pro-inflammatory cytokines and encourages M2 MØ polarization. Porro et al. reported that curcumin enhances the expression of SOCS-1 in microglia cells, thereby reducing neuroinflammation through suppression of the JAK2/STAT3 signaling pathway [37]. Wang et al. further showed that curcumin decreases neuroinflammation in a model of intracerebral hemorrhage by inactivating the JAK1/STAT1 pathway in M1 microglia [38]. Additional mechanisms include curcumin's antioxidant properties, which lower reactive oxygen species (ROS) levels and foster an environment conducive to M2 polarization [39,40]. Moreover, curcumin influences the expression of various microRNAs and small non-coding RNAs, further guiding MØ polarization towards the M2 phenotype through the modulation of these gene expressions [41,42].

To address the molecular mechanisms of nanocurcumin in zein nanofibers, it is important to emphasize the role of curcumin in modulating macrophage polarization and cytokine expression through multiple pathways. Nanocurcumin, by being encapsulated within zein nanofibers, may provide controlled and sustained release, enhancing bioavailability and stability of curcumin. This enhances its capacity to modulate the NF-κB pathway, leading to the reduction of pro-inflammatory cytokines such as IL-1β, IL-6, and TNF-α, while simultaneously activating the PPAR-γ pathway and suppressing the JAK/STAT signaling. These combined effects promote M2 macrophage polarization and anti-inflammatory cytokine production, which contribute to improved wound healing outcomes. Understanding these molecular interactions may inform the optimization of nanofiber design by refining the release profiles or enhancing the bioactivity of nanocurcumin.

Despite the promising findings of this study, several limitations should be acknowledged. First, the use of only male rats limits the generalizability of the results to both sexes. There are notable differences in the dermal and epidermal anatomy between male and female animals, which may influence treatment outcomes. Fluctuating hormone levels in females, especially due to estrous cycles, could potentially affect wound healing processes, including macrophage polarization and collagen deposition. Future studies should aim to include equal proportions of male and female animals to provide a more comprehensive understanding of treatment efficacy across sexes and enhance the generalizability of the results. Second, while this study effectively demonstrated the modulation of macrophage polarization through gene expression analysis of iNOS and Arg-1, no protein-level validation was performed to confirm these findings. The absence of techniques such as immunohistochemistry or western blotting limits the ability to verify the actual protein expression changes corresponding to the gene expression data. Further research should include these validation techniques to strengthen the evidence of the effects of Zein/nCUR nanofibers on macrophage polarization. Finally, this study focused on a single wound model in rats, which may not fully capture the complexity and diversity of wound healing in different conditions, such as chronic wounds or diabetic wounds. Additional studies using various wound models, including those with comorbidities, are necessary to better understand the broader potential applications of Zein/nCUR nanofibers in wound care. These limitations highlight the need for further research to refine our understanding and improve the clinical translation of these findings.

5. Conclusion

In conclusion, this study demonstrates that Zein/nCUR 10 % NFs possess the capability to shift MØs from the pro-inflammatory M1 phenotype to the reparative M2 phenotype, thereby reducing inflammation. Additionally, these nanofibers significantly enhance wound healing processes, including wound closure, collagen secretion, and re-epithelialization. These promising results lay the groundwork for the development of innovative therapeutic strategies designed to improve wound care and patient outcomes. The potential of Zein/nCUR 10 % NFs to modulate immune responses and promote tissue regeneration underscores their value in advancing wound healing technologies. While this study highlights the therapeutic potential of Zein/nCUR 10 % NFs, future work could focus on optimizing nanofiber design based on the molecular insights gained from the modulation of macrophage polarization. Adjusting nanocurcumin loading or fiber composition may further enhance these therapeutic effects. Strengths of this study include the detailed mechanistic analysis of immune modulation and wound healing, but limitations such as the lack of protein validation and use of only male rats should be addressed in future research to improve generalizability and clinical translation.

Ethics approval and consent to participate

The Bioethics Committee of Fasa University of Medical Sciences granted approval for all experimental procedures conducted in this study, as indicated by the assigned ethics code IR.FUMS.REC.1399.121. In conducting animal experiments, strict adherence to the ARRIVE (Animal Research: Reporting of In Vivo Experiments) guidelines was maintained to ensure ethical and transparent reporting. Furthermore, all procedures conformed to the standards set forth by the Animals (Scientific Procedures) Act 1986, including its associated guidelines, as well as the EU Directive 2010/63, which aims to protect animals utilized for scientific research purposes.

Availability of data and materials

All data generated during the current study are available from the corresponding author on reasonable request.

CRediT author statement

Mohammad Ebrahim Astaneh (Investigation, Writing - Review & Editing), and Narges Fereydouni (Conceptualization, Writing - Original Draft).

Funding

This research was supported by funding from the Fasa University of Medical Sciences. The purpose of writing this article is to fulfill the project requirements associated with grant number 99024 and adhere to the ethical standards outlined under approval code IR.FUMS.REC.1399.121.

Declaration of competing interest

The authors declare that they have no known competing financial interests or personal relationships that could have appeared to influence the work reported in this paper.

Acknowledgement

The authors express their sincere gratitude to the Fasa University of Medical Sciences for generously funding this study, which was crucial for the successful completion of this research.

References

[1] Peña OA, Martin P. Cellular and molecular mechanisms of skin wound healing. Nat Rev Mol Cell Biol 2024:599–616. https://doi.org/10.1038/s41580-024-00715-1.
[2] Louiselle AE, Niemiec SM, Zgheib C, Liechty KW. Macrophage polarization and diabetic wound healing. Transl Res 2021;236:109–16. https://doi.org/10.1016/j.trsl.2021.05.006.
[3] Aitcheson SM, Frentiu FD, Hurn SE, Edwards K, Murray RZ. Skin wound healing: normal macrophage function and macrophage dysfunction in diabetic wounds. Molecules 2021;26:4917. https://doi.org/10.3390/molecules26164917.
[4] Sharifiaghdam M, Shaabani E, Faridi-Majidi R, De Smedt SC, Braeckmans K, Fraire JC. Macrophages as a therapeutic target to promote diabetic wound healing. Mol Ther 2022;30:2891–908. https://doi.org/10.1016/j.ymthe.2022.07.016.
[5] Fu Y-S, Chen T-H, Weng L, Huang L, Lai D, Weng C-F. Pharmacological properties and underlying mechanisms of curcumin and prospects in medicinal potential. Biomed Pharmacother 2021;141:111888. https://doi.org/10.1016/j.biopha.2021.111888.
[6] Salehi B, Stojanović-Radić Z, Matejić J, Sharifi-Rad M, Kumar NVA, Martins N, et al. The therapeutic potential of curcumin: a review of clinical trials. Eur J Med Chem 2019;163:527–45. https://doi.org/10.1016/j.ejmech.2018.12.016.
[7] Urošević M, Nikolić L, Gajić I, Nikolić V, Dinić A, Miljković V. Curcumin: biological activities and modern pharmaceutical forms. Antibiotics 2022;11:135. https://doi.org/10.3390/antibiotics11020135.
[8] Slika L, Patra D. A short review on chemical properties, stability and nanotechnological advances for curcumin delivery. Expet Opin Drug Deliv 2020;17:61–75. https://doi.org/10.1080/17425247.2020.1702644.
[9] Zheng B, McClements DJ. Formulation of more efficacious curcumin delivery systems using colloid science: enhanced solubility, stability, and bioavailability. Molecules 2020;25:2791. https://doi.org/10.3390/molecules25122791.
[10] Tabanelli R, Brogi S, Calderone V. Improving curcumin bioavailability: current strategies and future perspectives. Pharmaceutics 2021;13:1715. https://doi.org/10.3390/pharmaceutics13101715.
[11] Fereydouni N, Darroudi M, Movaffagh J, Shahroodi A, Butler AE, Ganjali S, et al. Curcumin nanofibers for the purpose of wound healing. J Cell Physiol 2019;234:5537–54. https://doi.org/10.1002/jcp.27362.
[12] Rathinavel S, Korrapati PS, Kalaiselvi P, Dharmalingam S. Mesoporous silica incorporated PCL/Curcumin nanofiber for wound healing application. Eur J Pharmaceut Sci 2021;167:106021. https://doi.org/10.1016/j.ejps.2021.106021.
[13] Chen K, Pan H, Ji D, Li Y, Duan H, Pan W. Curcumin-loaded sandwich-like nanofibrous membrane prepared by electrospinning technology as wound dressing for accelerate wound healing. Mater Sci Eng C 2021;127:112245. https://doi.org/10.1016/j.msec.2021.112245.
[14] Prakash J, Venkataprasanna K, Bharath G, Banat F, Niranjan R, Venkatasubbu GD. In-vitro evaluation of electrospun cellulose acetate nanofiber containing Graphene oxide/TiO2/Curcumin for wound healing application. Colloids Surf A Physicochem Eng Asp 2021;627:127166. https://doi.org/10.1016/j.colsurfa.2021.127166.
[15] Tamilarasi GP, Krishnan M, Sabarees G, Gouthaman S, Alagarsamy V, Solomon VR. Emerging trends in curcumin embedded electrospun nanofibers for impaired diabetic wound healing. Appl Nanosci 2022;3:202–32. https://doi.org/10.3390/applnano3040015.
[16] Golchin A, Hosseinzadeh S, Jouybar A, Staji M, Soleimani M, Ardeshirylajimi A, et al. Wound healing improvement by curcumin-loaded electrospun nanofibers and BFP-MSCs as a bioactive dressing. Polym Adv Technol 2020;31:1519–31. https://doi.org/10.1002/pat.4881.
[17] Fereydouni N, Movaffagh J, Amiri N, Darroudi S, Gholoobi A, Goodarzi A, et al. Synthesis of nano-fibers containing nano-curcumin in zein corn protein and its physicochemical and biological characteristics. Sci Rep 2021;11:1902. https://doi.org/10.1038/s41598-020-73678-w.
[18] Moghaddasi F, Housaindokht MR, Darroudi M, Bozorgmehr MR, Sadeghi A. Synthesis of nano curcumin using black pepper oil by O/W Nanoemulsion Technique and investigation of their biological activities. LWT 2018;92:92–100. https://doi.org/10.1016/j.lwt.2018.02.023.
[19] Dunn L, Prosser HC, Tan JT, Vanags LZ, Ng MK, Bursill CA. Murine model of wound healing. JoVE (J Visual Exp) 2013:e50265. https://doi.org/10.3791/50265.
[20] Birch M, Tomlinson A, Ferguson MW. Animal models for adult dermal wound healing. Fibrosis Res 2005;(223):223–35. https://doi.org/10.1385/1-59259-940-0. Springer.
[21] Dalirfardouei R, Jamialahmadi K, Jafarian AH, Mahdipour E. Promising effects of exosomes isolated from menstrual blood-derived mesenchymal stem cell on wound-healing process in diabetic mouse model. J Tiss Eng Regenerat Med 2019;13:555–68. https://doi.org/10.1002/term.2799.
[22] Mo Z, Yuan J, Guan X, Peng J. Advancements in dermatological applications of curcumin: clinical efficacy and mechanistic insights in the management of skin disorders. Clin Cosmet Invest Dermatol 2024:1083–92. https://doi.org/10.2147/CCID.S467442.
[23] Singh H, Dhanka M, Yadav I, Gautam S, Bashir SM, Mishra NC, et al. Technological interventions enhancing curcumin bioavailability in wound-healing therapeutics. Tissue Eng B Rev 2024;30:230–53. https://doi.org/10.1089/ten.TEB.2023.0085.
[24] Abdollahi E, Johnston TP, Ghaneifar Z, Vahedi P, Goleij P, Azhdari S, et al. Immunomodulatory therapeutic effects of curcumin on M1/M2 macrophage polarization in inflammatory diseases. Curr Mol Pharmacol 2023;16:2–14. https://doi.org/10.2174/1874467215666220324114624.
[25] Berbudi A, Anshori H, Andromeda A, Kwarteng A, Putri AC, Atik N. Topical administration of Curcuma longa L. extract gel increases M2 macrophage polarization and collagen density in skin excision. J Appl Pharmaceut Sci 2021;11:95–100. https://doi.org/10.7324/JAPS.2021.110111.
[26] Dehghani S, Dalirfardouei R, Jafari Najaf, Abadi MH, Ebrahimi Nik M, Jaafari MR, et al. Topical application of curcumin regulates the angiogenesis in diabetic-impaired cutaneous wound. Cell Biochem Funct 2020;38:558–66. https://doi.org/10.1002/cbf.3500.
[27] Al Sadoun H. Macrophage phenotypes in normal and diabetic wound healing and therapeutic interventions. Cells 2022;11:2430. https://doi.org/10.3390/cells11152430.
[28] Willenborg S, Injarabian L, Eming SA. Role of macrophages in wound healing. Cold Spring Harbor Perspect Biol 2022;14:a041216. https://doi.org/10.1101/cshperspect.a041216.
[29] Raziyeva K, Kim Y, Zharkinbekov Z, Kassymbek K, Jimi S, Saparov A. Immunology of acute and chronic wound healing. Biomolecules 2021;11:700. https://doi.org/10.3390/biom11050700.
[30] Hassanshahi A, Moradzad M, Ghalamkari S, Fadaei M, Cowin AJ, Hassanshahi M. Macrophage-mediated inflammation in skin wound healing. Cells 2022;11:2953. https://doi.org/10.3390/cells11192953.
[31] Kuraitis D, Rosenthal N, Boh E, McBurney E. Macrophages in dermatology: pathogenic roles and targeted therapeutics. Arch Dermatol Res 2022:20221–8. https://doi.org/10.1007/s00403-021-02207-0.
[32] Ran Y, Su W, Gao F, Ding Z, Yang S, Ye L, et al. Curcumin ameliorates white matter injury after ischemic stroke by inhibiting microglia/macrophage pyroptosis through NF-κB suppression and NLRP3 inflammasome inhibition. Oxid Med Cell Longev 2021;2021:1552127. https://doi.org/10.1155/2021/1552127.
[33] Lee MK, Kim HD, Lee SH, Lee JH. Curcumin ameliorates particulate matter-induced pulmonary injury through bimodal regulation of macrophage inflammation via NF-κB and Nrf2. Int J Mol Sci 2023;24:1858. https://doi.org/10.3390/ijms24031858.
[34] Chen D, Xi Y, Zhang S, Weng L, Dong Z, Chen C, et al. Curcumin attenuates inflammation of Macrophage-derived foam cells treated with Poly-L-lactic acid degradation via PPARγ signaling pathway. J Mater Sci Mater Med 2022;33:33. https://doi.org/10.1007/s10856-022-06654-7.
[35] Hu Q, Bian Q, Rong D, Wang L, Song J, Huang H-S, et al. JAK/STAT pathway: extracellular signals, diseases, immunity, and therapeutic regimens. Front Bioeng Biotechnol 2023;11:1110765. https://doi.org/10.3389/fbioe.2023.1110765.
[36] Sarapultsev A, Gusev E, Komelkova M, Utepova I, Luo S, Hu D. JAK-STAT signaling in inflammation and stress-related diseases: implications for therapeutic interventions. Mol Biomed 2023;4:40. https://doi.org/10.1186/s43556-023-00151-1.

[37] Porro C, Cianciulli A, Trotta T, Lofrumento DD, Panaro MA. Curcumin regulates anti-inflammatory responses by JAK/STAT/SOCS signaling pathway in BV-2 microglial cells. Biology 2019;8:51. https://doi.org/10.3390/biology8030051.

[38] Wang F, Xia J-j, Shen L-j, Jiang T-t, Li W-l, You D-L, et al. Curcumin attenuates intracerebral hemorrhage-induced neuronal apoptosis and neuroinflammation by suppressing JAK1/STAT1 pathway. Biochem Cell Biol 2022;100:236–45. https://doi.org/10.1139/bcb-2021-0423.

[39] Momtazi-Borojeni AA, Abdollahi E, Nikfar B, Chaichian S, Ekhlasi-Hundrieser M. Curcumin as a potential modulator of M1 and M2 macrophages: new insights in atherosclerosis therapy. Heart Fail Rev 2019;24:399–409. https://doi.org/10.1007/s10741-018-09764-z.

[40] Nasra S, Shah T, Bhatt M, Chaudhari R, Bhatia D, Kumar A. Reprogramming M1-to-M2 phenotype to alleviate inflammation: using liposomal curcumin as a tool to redefine macrophage functionality. ACS Appl Bio Mater 2023;6:2886–97. https://doi.org/10.1021/acsabm.3c00316.

[41] Tan C, Zhou L, Wen W, Xiao N. Curcumin promotes cholesterol efflux by regulating ABCA1 expression through miR-125a-5p/SIRT6 axis in THP-1 macrophage to prevent atherosclerosis. J Toxicol Sci 2021;46:209–22. https://doi.org/10.2131/jts.46.209.

[42] Zhong Y, Liu C, Feng J, Li J, Fan Z. Curcumin affects oxLDLinduced IL6, TNFα, MCP1 secretion and cholesterol efflux in THP1 cells by suppressing the TLR4/NFκB/miR33a signaling pathway. Exp Ther Med 2020;20:1856–70. https://doi.org/10.3892/etm.2020.8915.